

Generating Spatially-Variant Metamaterial Lattices Designed from Spatial Transforms

Eric A. Berry and Raymond C. Rumpf*

Abstract—Spatial transform techniques like transformation optics and conformal mapping have arisen as the dominant techniques for designing metamaterial devices. However, these techniques only produce the electrical permittivity and permeability as a function of position. The manner in which these functions are converted into physical metamaterial lattices remains elusive, except in some simple or canonical configurations. Metamaterial lattices designed by spatial transforms are composed of elements of different sizes, orientations, and designs. The elements must be distributed and oriented in a manner that makes the final lattice smooth, continuous, have uniform density, be free of unintentional defects, and have minimal distortions to the elements. Any of these would weaken or destroy the electromagnetic properties of the lattice. This paper describes a general purpose method to generate such arbitrary metamaterial lattices. Inputs to the algorithm are the permittivity and permeability functions as well as the baseline metamaterials that can provide the necessary permittivity and permeability values. In prior research, we reported a simple finite-difference technique for calculating the permittivity and permeability functions for arbitrary shaped devices using transformation optics. The methodology presented in this work is illustrated by generating an electromagnetic cloak of arbitrary shape that was designed using the previously reported technique. The final metamaterial cloak is simulated using the finite-difference time-domain method and performance compared to other cloaks reported in the literature.

1. INTRODUCTION

Spatial transform techniques, like transformation optics (TO) and conformal mapping, use coordinate transforms to sculpt electromagnetic fields and direct the flow of waves within a device [1–3]. All of these techniques aim to encapsulate the effects of the spatial transformation into the material properties of the device. The output of these methods are permittivity and permeability as a function of position, that if realized would sculpt the fields and direct the flow of waves according to the original transform. This level of control over the electromagnetic fields allows devices such as cloaks [4–9], lenses [10, 11], tight bends [12], beam splitters [2, 13, 14], concentrators [8, 15, 16], and many others [2] to be designed.

The vast majority of devices designed to date using TO have been derived using analytical expressions [2, 17]. Analytical expressions, however, are fundamentally limited in the coordinate transforms they can describe. In prior research, based in part on Ref. [18], we developed a fully numerical technique for implementing TO that is able to design devices of any shape defined only by its boundaries [19]. Figure 1(a) shows the boundaries of an arbitrary electromagnetic cloak. The permittivity and permeability tensors for this device were calculated using this approach. The permittivity and permeability functions that come from TO are generally fully anisotropic tensors [20]. To physically realize such materials, it is necessary to determine a coordinate system in which the tensors can be represented as diagonal matrices.

Received 30 October 2019, Accepted 27 April 2020, Scheduled 10 May 2020

* Corresponding author: Raymond C. Rumpf (rcrumpf@utep.edu).

The authors are with the EM Lab, University of Texas at El Paso, USA.

To manufacture a device designed using TO, materials must be obtained which have the same electromagnetic response as that of the material tensors derived from TO. The permittivity and permeability values that come out of TO are typically not achievable using naturally occurring materials [4, 21]. Metamaterials are currently the best option for realizing the required material properties [22, 23]. However, it is often still not possible to realize the most extreme constitutive values. In some cases, it is possible to simplify the operating parameters for the device in order to mitigate the most extreme material properties. For the electromagnetic cloak shown in Figure 1 the device was designed to operate at 12 GHz for an electric field polarized in the positive z direction. Restricting the polarization in this manner allows the material properties to be simplified in the same manner as described in Ref. [17] to only require three tensor components rather than the entire permittivity and permeability tensors. If other polarizations are desired, metamaterial selection and parameter retrieval

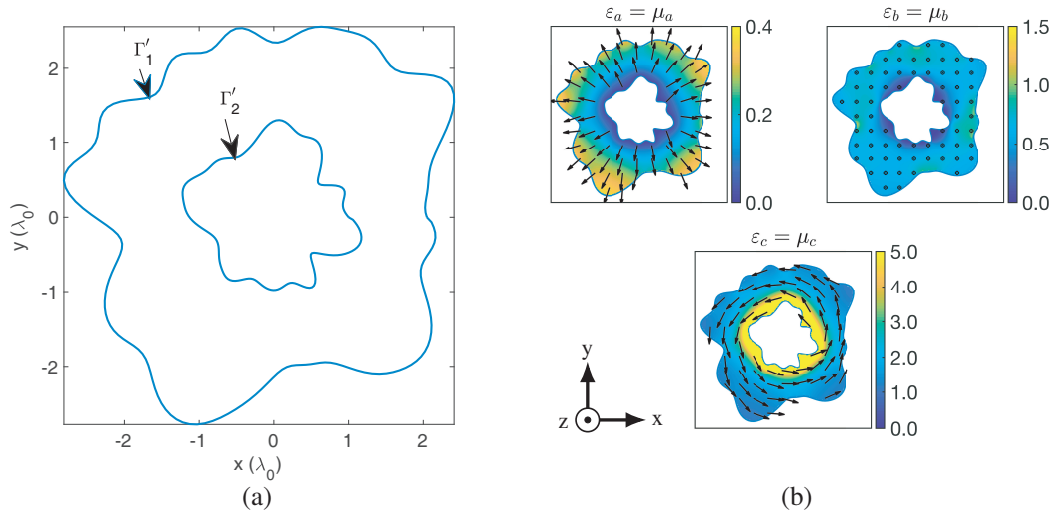


Figure 1. (a) Boundaries of an arbitrary TO cloak designed. (b) Diagonalized permittivity and permeability tensors calculated using approach in Ref. [19].

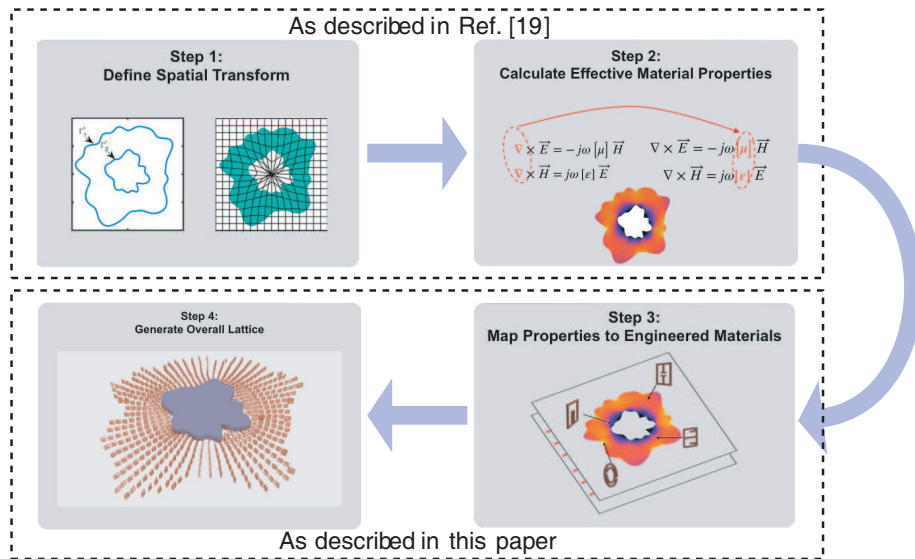


Figure 2. Block diagram of metamaterial design process using TO and spatially-variant lattices to generate the physical lattice of the device.

methods must take these polarizations into consideration. However, for the intent of demonstrating the lattice synthesis techniques described in this paper, those discussions are beyond the scope of this article.

The overall methodology presented in this paper is summarized in Figure 2. As described in Ref. [19], the spatial variation shown in Step 1 is generated by calculating a coordinate transformation based on solving Laplace’s equation for an arbitrary boundary value problem. Step 2 is implemented using the equations of TO with the numerically generated coordinate transformation from Step 1. This paper will focus on the bottom half of Figure 2. The material tensors derived in Step 2 are assigned to metamaterials based on the response necessary. The proper scaling for the metamaterial is chosen by optimization to match the effective material properties throughout the device. The metamaterial elements are then placed in the device by using a spatially-variant lattice to ensure that the arrangement of elements is smooth, continuous, and free of defects.

2. MAP PERMITTIVITY AND PERMEABILITY TO ENGINEERED MATERIALS

2.1. Tensor Diagonalization

The orientation of the coordinate system in which the off-diagonal tensor elements vanish is known as the principal axes of the material [24, 25]. The principal axes and the diagonalized constitutive values can be determined by solving an eigenvalue problem [24, 26, 27] throughout the device. The eigenvalues are the permittivity or permeability in the direction of the associated eigenvector. The eigenvectors are known as the principal axes of the anisotropic material. Figure 1(b) shows the diagonalized material tensor for the cloak where the vectors \hat{a} , \hat{b} , and \hat{c} are the principal axes of the material tensors.

2.2. Metamaterial Mapping

Given the diagonalization information discussed in the previous section, it is necessary to identify metamaterial element designs that can realize the constitutive values at each point in the device. For illustration purposes, the present work utilized the magnetic-electric LC (MELC) structure presented in Ref. [28] because it is highly resonant it provides a wide range of values applicable to this device, but at a single frequency with negligible bandwidth. The metamaterial element is shown in Figure 3.

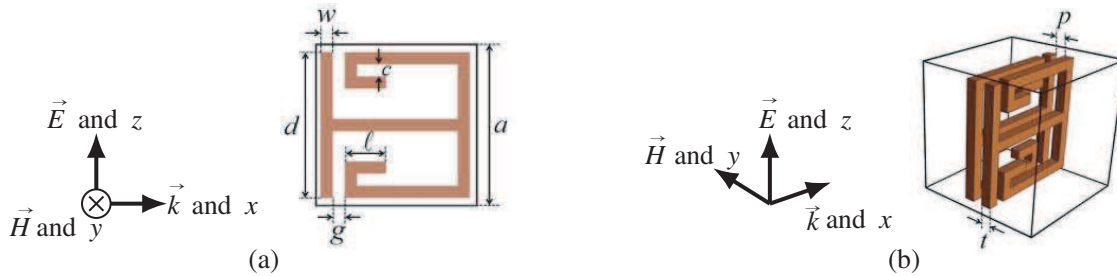


Figure 3. (a) MELC unit cell with the dimensions $d = 3.0$ mm, $w = 0.25$ mm, $g = 0.25$ mm, $l = 0.6$ mm, $c = 0.25$ mm. (b) The spacing between structures is $p = 0.25$ mm and the conductor thickness is $t = 0.25$ mm.

To determine the full range of constitutive values made possible by our choice of metamaterial element, a parameter sweep was performed to calculate the constitutive values as a function of scale. The scale in the x and z directions was swept from 0.01 times the nominal dimensions to 1.0 times the nominal dimensions in 0.01 increments using Ansys Electronics Workbench [29]. After parameter retrieval [30–33], a two dimensional map of both the permittivity and permeability, the real part of which is shown in Figure 4, were generated as a function of the scaling of each structure shown in Figure 3(b). The variables Scale1 and Scale2 were the scaling value for the structure in the negative and positive y direction respectively.

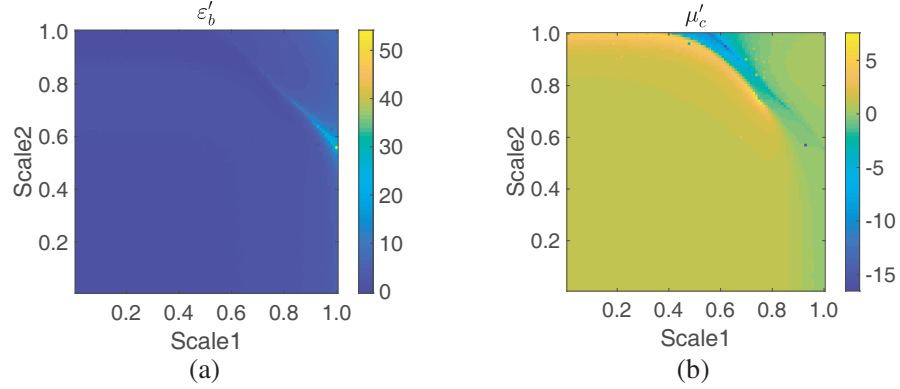


Figure 4. Parameter retrieval maps of ε_z and μ_y for the metamaterial shown in Figure 3.

Given the constitutive values as a function of scale, we calculated the scale of the metamaterial element throughout the device that would best realize the required values for permittivity and permeability. It was not possible to achieve an exact match so the scales were chosen to minimize the error term δ in Eq. (1) at each point (i, j) throughout the device material maps. Other optimization techniques such as genetic algorithm (GA) [34, 35] or particle swarm optimization (PSO) [36] can be used to select the optimal metamaterial scales. For the cloak shown in Figure 1 simplified for a z polarized electric field, as described previously, the constitutive material values of concern are ε_b and μ_c from Figure 1(b).

$$\delta(i, j) = |\varepsilon_b(i, j) - \varepsilon'_z| + |\mu_c(i, j) - \mu'_y| \quad (1)$$

Figure 5 shows the final mapping used for the electromagnetic cloak. The terms labeled “Fit μ_c ” and “Fit ε_c ” are actual constitutive values that are realized by scaling the MELC element. This is not an exact match to what is prescribed by TO so an electromagnetic simulation was performed using an anisotropic finite-difference frequency-domain (AFDFD) method [19, 37]. The results of this simulation are presented in a later section.

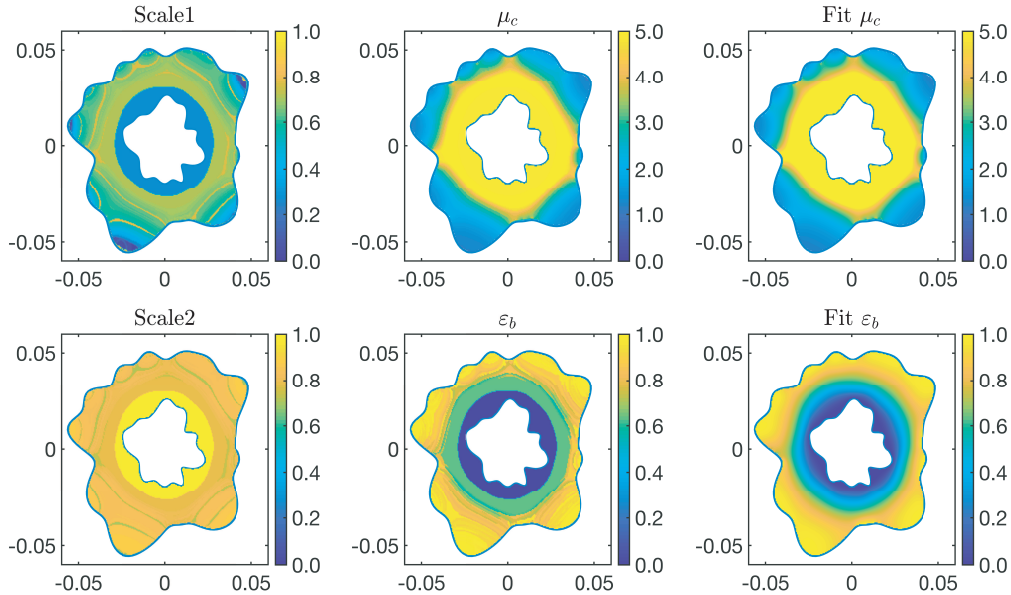


Figure 5. Device mapping with scale values in the left column, constitutive parameters of the device from TO in the center column, and constitutive parameter of the scaled metamaterial in the right column.

3. GENERATING SPATIALLY-VARIANT METAMATERIAL LATTICES

3.1. Generating Spatially-Variant Lattices On Nonuniform Grids

Given the metamaterial elements and their scaling and orientation as a function of position, it is necessary to determine where the elements should be placed. These locations should be chosen in a manner that gives a smooth lattice, avoids defects, and maintains a uniform density of elements throughout the device despite the variations in size, geometry, and spacing. A method for doing this was developed by modifying a previously reported algorithm for generating spatially-variant lattices [38–41]. The original algorithm decomposes the unit cells into a set of planar gratings which are each spatially varied throughout the device and then added to get the final lattice. The metamaterial elements used for this research would require many thousands of spatial harmonics to resolve the very fine features of the metallic elements. As a faster alternative, two planar gratings were spatially varied to follow the principle axes of the metamaterials and to accommodate variations in element size. The metamaterial elements were then placed at the intersections of these two planar gratings. This alternative approach required a nonuniform and circulating grid that conformed to the boundaries of the cloak, as shown in Figure 6.

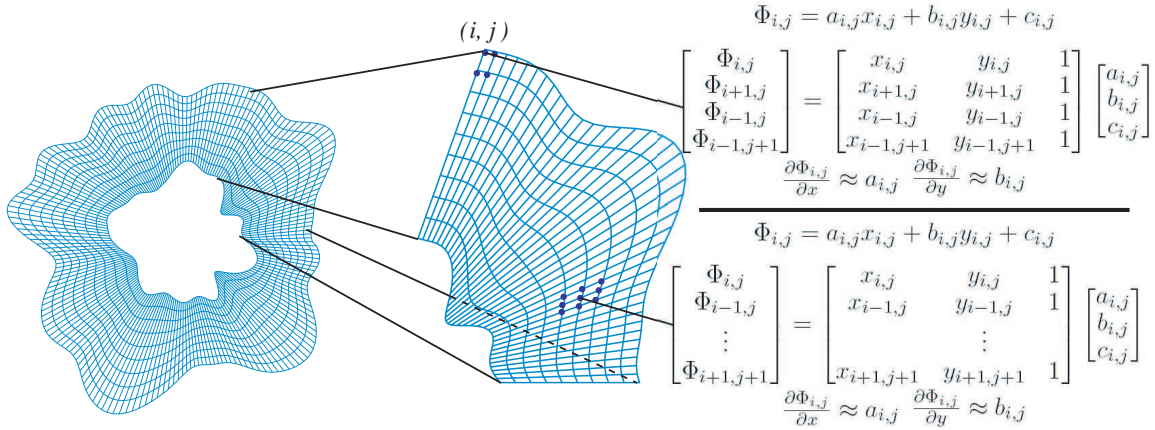


Figure 6. Solving $\nabla\Phi = \vec{K}$ on a nonuniform spatially-variant grid.

The algorithm for spatially varying a single planar grating begins by defining its grating vector function $\vec{K}(\vec{r})$, or K -function. The K -function is a vector function that conveys both the orientation and period of the grating. The direction of the K -function is set equal to one of the principle axes of the diagonalized tensors throughout the lattice. The magnitude of the K -function is set to 2π divided by the scale of the MELC elements throughout the lattice. Given this, the grating phase throughout the device is calculated by solving Eq. (2) for $\Phi(\vec{r})$.

$$\nabla\Phi(\vec{r}) = \vec{K}(\vec{r}) \quad (2)$$

Following the procedure outlined in Ref. [39], the solution can be obtained using the finite-difference method. In finite-difference form, Eq. (2) can be expressed in two-dimensions as

$$\begin{bmatrix} \mathbf{D}_x \\ \mathbf{D}_y \end{bmatrix} \Phi = \begin{bmatrix} \mathbf{k}_x \\ \mathbf{k}_y \end{bmatrix} \quad (3)$$

where \mathbf{D}_x , and \mathbf{D}_y are square derivative matrices, and \mathbf{k}_x and \mathbf{k}_y are column vectors containing the components of the K -function throughout the entire grid. In the modified algorithm, however, the finite-difference operators \mathbf{D}_x and \mathbf{D}_y must be constructed to operate on a nonuniform grid. An array is constructed of all of the x and y coordinates of the grid. Considering the cutaway section of the grid shown in Figure 6, the grating phase at each point corresponding to the array indices (i, j) on the grid can be fit to the following linear function


$$\Phi_{i,j}(x, y) = a_{i,j}x + b_{i,j}y + c_{i,j} \quad (4)$$

Deriving the first-derivative of Eq. (4) with respect to x and then to y leads to

$$\frac{\partial \Phi_{i,j}(x,y)}{\partial x} = a_{i,j} \qquad \frac{\partial \Phi_{i,j}(x,y)}{\partial y} = b_{i,j} \quad (5)$$

The coefficients $a_{i,j}$, $b_{i,j}$, and $c_{i,j}$ are determined in Eq. (5) by solving a small matrix equation formed by writing Eq. (4) for the $M * N$ points in the vicinity of the point designated by the element (i, j) . For points that are evaluated on the boundary of the grid only those points which are neighboring are used to form the matrix equation as illustrated in Figure 6. The solution in Eq. (5) requires the use of a pseudoinverse [42].

pseudoinverse



$$\begin{bmatrix} \Phi_{i,j} \\ \Phi_{i-1,j} \\ \vdots \\ \Phi_{M,N} \end{bmatrix} = \begin{bmatrix} x_{i,j} & y_{i,j} & 1 \\ x_{i-1,j} & y_{i-1,j} & 1 \\ & \vdots & \\ x_{M,N} & y_{M,N} & 1 \end{bmatrix} \begin{bmatrix} a_{i,j} \\ b_{i,j} \\ c_{i,j} \end{bmatrix} \longrightarrow \begin{bmatrix} a_{i,j} \\ b_{i,j} \\ c_{i,j} \end{bmatrix} = \begin{bmatrix} \alpha_{i,j} & \alpha_{i-1,j} & \dots & \alpha_{M,N} \\ \beta_{i,j} & \beta_{i-1,j} & \dots & \beta_{M,N} \\ \gamma_{i,j} & \gamma_{i-1,j} & \dots & \gamma_{M,N} \end{bmatrix} \begin{bmatrix} \Phi_{i,j} \\ \Phi_{i-1,j} \\ \vdots \\ \Phi_{M,N} \end{bmatrix} \quad (6)$$

Substituting the expressions for $a_{i,j}$ and $b_{i,j}$ into Eq. (5), the following expressions are derived.

$$\frac{\partial \Phi_{i,j}(x,y)}{\partial x} = a_{i,j} \approx \alpha_{i,j} \Phi_{i,j} + \alpha_{i-1,j} \Phi_{i-1,j} + \dots + \alpha_{M,N} \Phi_{M,N} \quad (7)$$

$$\frac{\partial \Phi_{i,j}(x,y)}{\partial y} = b_{i,j} \approx \beta_{i,j} \Phi_{i,j} + \beta_{i-1,j} \Phi_{i-1,j} + \dots + \beta_{M,N} \Phi_{M,N} \quad (8)$$

where α and β are the components of the first and second rows respectively of the pseudoinverse matrix in Eq. (6). The finite-difference matrices \mathbf{D}_x and \mathbf{D}_y in Eq. (3) are constructed by placing the values of α and β in the i^{th} row in the columns corresponding to the positions $x_{i,j}$ and $y_{i,j}$.

With the derivative matrices and grating vectors constructed, the grating phase Φ is found by solving the equation

$$\Phi = \begin{bmatrix} \mathbf{D}_x \\ \mathbf{D}_y \end{bmatrix}^{-1} \begin{bmatrix} \mathbf{k}_x \\ \mathbf{k}_y \end{bmatrix} \quad (9)$$

using least squares [43].

3.2. Metamaterial Lattice Construction

To determine the position and spacing of the metamaterial elements which will compose the device described thus far, Eq. (9) is solved for both the \hat{a} and \hat{c} principal axes. Figure 7 shows the planar gratings generated from the procedures described in the previous section and Ref. [38]. Figure 7(c) is the sum of the \hat{a} and \hat{c} directed planar gratings which is used to determine the points of intersection of the two gratings.

The intersection of the two planar gratings determined the position of the metamaterials in the device and the orientation of the metamaterial element was determined by interpolating the angle of principal axes at the position where the element was placed. Likewise, the scaling for the metamaterial element was calculated by interpolating the scales resulting from the material mapping to the metamaterial element position.

From there, the algorithm iterated through each point identified as an intersection of the two planar gratings. A surface mesh of the basic MELC elements was generated as a list of faces and vertices. The mesh was scaled to the appropriate size at the point to give the desired permittivity and permeability. The mesh was then rotated using rotation matrices to put the mesh in the correct orientation. Last, the mesh was shifted so as to be centered at the point. At the end, all of these meshes were combined into a single mesh and saved as standard tessellation language (STL) file common in the 3D printing industry. The final device with all the elements positioned properly is shown in Figure 8.

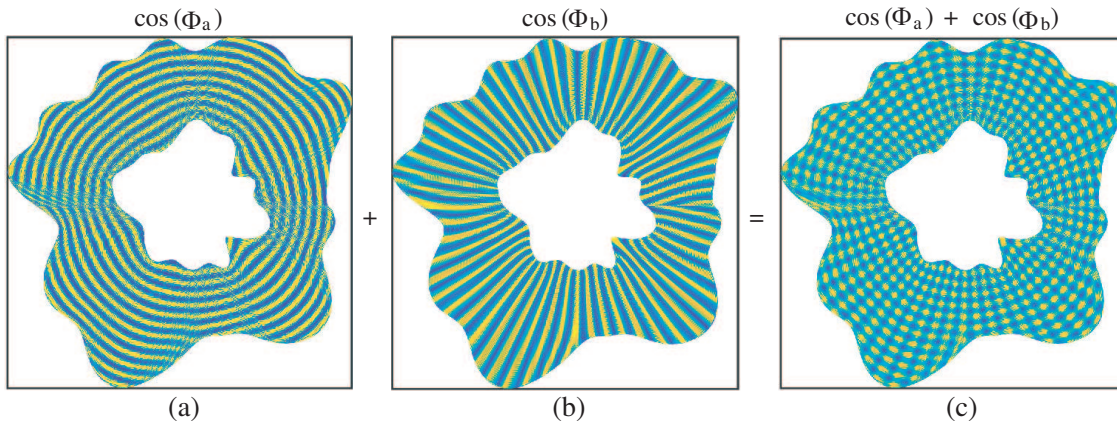


Figure 7. Planar gratings generated by solving Eq. (3) for both the \hat{a} (a) and \hat{c} (b) principal axes. (c) Sum of the planar gratings in (a) and (b) used to determine points of intersection between the gratings.



Figure 8. Cloak generated using the metamaterial elements shown in Figure 3 and spatially varied according using the lattice generated in Figure 7.

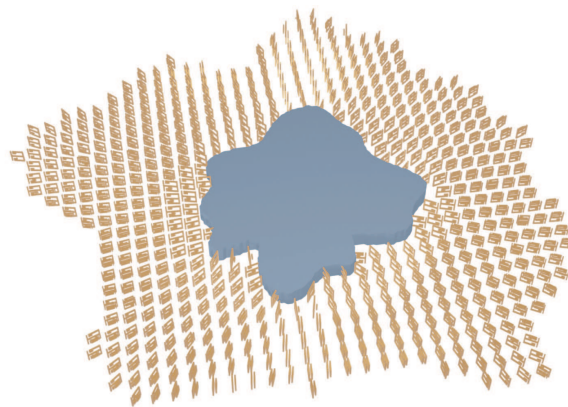


Figure 9. Transformation optics cloak with metamaterial elements arranged using a masked uniform Cartesian lattice.

To illustrate the benefit of using a spatially-variant lattice, the device designed above was also implemented using a Cartesian grid. First, a uniform lattice of points spaced with the lattice spacing of the nominal MELC unit cell (3.333 mm) was created. This uniform lattice was masked with the outline of the cloaking device being designed. Using the algorithm described previously in this chapter, the position, orientation, and scaling were determined on the Cartesian lattice. The metamaterial elements were placed uniformly on the Cartesian grid and the resulting device is shown in Figure 9. The Cartesian cloak has two deficiencies when compared to the device designed using the spatially-variant lattice. First, the spatially-variant lattice conforms to the boundaries of the cloak, whereas the Cartesian cloak has very sharp features because of the rectangular grid on which the materials are placed. Another drawback of the Cartesian device is that the effective material properties of the metamaterial elements are diluted when they undergo a rotation. This is because the Cartesian grid does not compensate for the rotation of the unit cell, but only the material elements. The rotation of the metamaterial unit cells is accounted for in the construction of the spatially-variant lattice, therefore the spatially-variant lattice eliminates overlapping unit cells, while the Cartesian device has unit cells which overlap in some positions.

4. SIMULATIONS

Figure 10 shows the anisotropic finite-difference frequency-domain (AFDFD) [37] simulation of the device using only the real part of the metamaterial parameters.

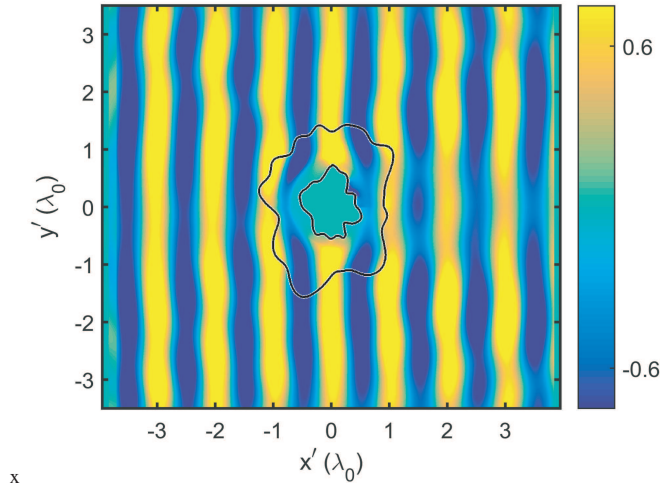


Figure 10. AFDFD simulation of the cloak with only the real part of the material parameters used.

To verify the effectiveness of the metamaterial cloak shown in Figure 8, a means of simulating the entire structure was necessary. The finite-difference time-domain (FDTD) method was chosen because the memory required for simulating large grids is much lower than other methods such as finite element method (FEM) and FDFD. FDTD was used to perform the simulation of the discrete element cloak shown in Figure 8. The STL file created for the device was imported as a finite difference mesh and a uniaxial perfectly matched layer boundary condition [44] was applied on all boundaries of the grid. A cross section of the electric field from this simulation is provided in Figure 11. The final device did not perform nearly as cleanly as the effective media cloak shown in Figure 10. Through simulation, this was found to be primarily due to the losses inherent in the metamaterial unit cells. This same problem can be seen in the cloak designed in Ref. [17], highlighting the limitations of currently existing metamaterial elements.

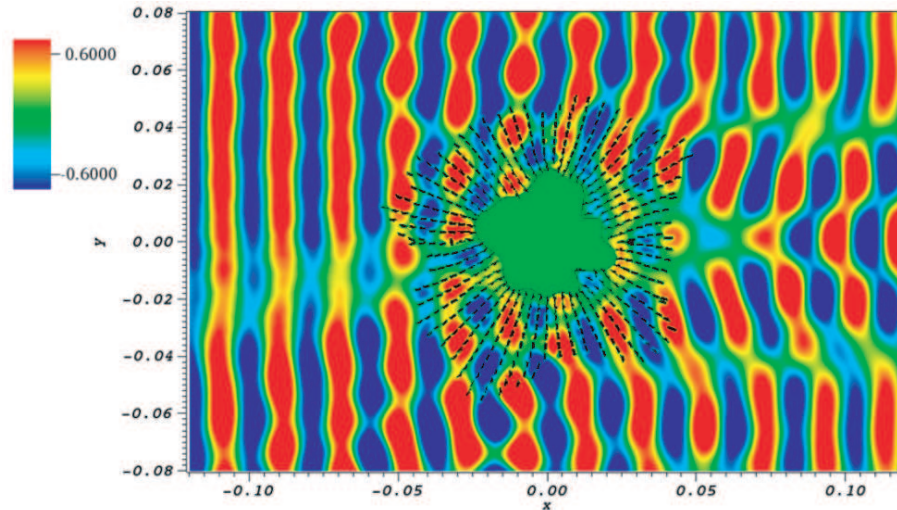


Figure 11. FDTD simulation of cloak shown in Figure 8.

5. CONCLUSION

The ability to spatially vary metamaterials to implement transformation electromagnetic devices will allow devices to be designed that are currently not realizable. Building upon the techniques presented previously in Ref. [19] to generate transformation optics devices numerically using a simple finite-difference method, the transformation media for a device to be designed can be determined using a fully numerical approach. This method makes it possible to design devices with arbitrary geometries defined only by the device boundaries. Additionally, the tools to simulate the effective media model of the device using the finite-difference time-domain and the anisotropic finite-difference frequency-domain methods [19] were discussed.

A method of determining the scaling for each metamaterial element corresponding to the material parameter to be represented was discussed within the context of designing an arbitrary metamaterial cloak to demonstrate the toolchain presented. Spatially-variant lattices were discussed as a method of placing the discrete metamaterial elements within the lattice in a manner which preserves the electromagnetic properties of the metamaterial unit cells. This technique allows devices to be constructed using metamaterial atoms that vary in size throughout the grid. The positions of the metamaterial elements are determined by calculating the intersections of the spatially-variant lattice. The orientation and scale of the elements are calculated by interpolating the values found by the metamaterial mapping operation and principal axes to the position identified by the intersection of the gratings. The final device designed using this method is then simulated using FDTD.

While the method presented in this research will produce a device based on the material parameters determined through transformation optics, the effectiveness of such a device is limited by the metamaterials which are available to implement it. As metamaterials are designed with more bandwidth and lower loss, the range of applications will expand as will their efficiency.

REFERENCES

1. Pendry, J. B., D. Schurig, and D. R. Smith, "Controlling electromagnetic fields," *Science*, 1780–2, New York, N.Y., Vol. 312, Jun. 2006.
2. Kwon, D.-H. and D. H. Werner, "Transformation electromagnetics: An overview of the theory and applications," *IEEE Antennas and Propagation Magazine*, Vol. 52, No. 1, 24–46, 2010.
3. Leonhardt, U. and T. G. Philbin, "Transformation optics and the geometry of light," *Progress in Optics*, Vol. 53, No. 08, 69–152, 2009.

4. Valentine, J., J. Li, T. Zentgraf, G. Bartal, and X. Zhang, "An optical cloak made of dielectrics," *Nature Materials*, Vol. 8, No. 7, 568, 2009.
5. Ergin, T., N. Stenger, Brenner, J. B. Pendry, and M. Wegener, "Three-dimensional invisibility cloak at optical wavelengths," *Science*, 1186351, 2010.
6. Gabrielli, L. H., J. Cardenas, C. B. Poitras, and M. Lipson, "Silicon nanostructure cloak operating at optical frequencies," *Nature Photonics*, Vol. 3, No. 8, 461, 2009.
7. Liu, R., C. Ji, J. Mock, J. Chin, T. Cui, and D. Smith, "Broadband ground-plane cloak," *Science*, Vol. 323, No. 5912, 366–369, 2009.
8. Rahm, M., D. Schurig, D. A. Roberts, S. A. Cummer, D. R. Smith, and J. B. Pendry, "Design of electromagnetic cloaks and concentrators using form-invariant coordinate transformations of Maxwell's equations," *Photonics and Nanostructures-fundamentals and Applications*, Vol. 6, No. 1, 87–95, 2008.
9. Li, J. and J. B. Pendry, "Hiding under the carpet: a new strategy for cloaking," *Physical Review Letters*, Vol. 101, No. 20, 203901, 2008.
10. Ma, H. F. and T. J. Cui, "Three-dimensional broadband and broad-angle transformation-optics lens," *Nature communications*, Vol. 1, 124, 2010.
11. Roberts, D., N. Kundtz, and D. Smith, "Optical lens compression via transformation optics," *Optics Express*, Vol. 17, No. 19, 16535–16542, 2009.
12. Rahm, M., D. Roberts, J. Pendry, and D. Smith, "Transformation-optical design of adaptive beam bends and beam expanders," *Optics Express*, Vol. 16, No. 15, 11555–11567, 2008.
13. Rahm, M., S. A. Cummer, D. Schurig, J. B. Pendry, and D. R. Smith, "Optical design of reflectionless complex media by finite embedded coordinate transformations," *Physical Review Letters*, Vol. 100, No. 6, 063903, 2008.
14. Kwon, D.-H. and D. H. Werner, "Polarization splitter and polarization rotator designs based on transformation optics," *Optics Express*, Vol. 16, No. 23, 18731–18738, 2008.
15. Jiang, W. X., T. J. Cui, Q. Cheng, J. Y. Chin, X. M. Yang, R. Liu, and D. R. Smith, "Design of arbitrarily shaped concentrators based on conformally optical transformation of nonuniform rational b-spline surfaces," *Applied Physics Letters*, Vol. 92, No. 26, 264101, 2008.
16. Yang, J., M. Huang, C. Yang, Z. Xiao, and J. Peng, "Metamaterial electromagnetic concentrators with arbitrary geometries," *Optics Express*, Vol. 17, No. 22, 19656–19661, 2009.
17. Schurig, D., J. Mock, B. Justice, S. A. Cummer, J. B. Pendry, A. Starr, and D. Smith, "Metamaterial electromagnetic cloak at microwave frequencies," *Science*, Vol. 314, No. 5801, 977–980, 2006.
18. Hu, J., X. Zhou, and G. Hu, "Design method for electromagnetic cloak with arbitrary shapes based on laplace's equation," *Optics express*, Vol. 17, No. 3, 1308–1320, 2009.
19. Berry, E. A., J. J. Gutierrez, and R. C. Rumpf, "Design and simulation of arbitrarily-shaped transformation optic devices using a simple finite-difference method," *Progress In Electromagnetics Research*, Vol. 68, 1–16, 2016.
20. Chen, H., C. T. Chan, and Sheng, "Transformation optics and metamaterials," *Nature Materials*, Vol. 9, No. 5, 387, 2010.
21. Mei, Z.-L., J. Bai, T. M. Niu, and T.-J. Cui, "A planar focusing antenna design with the quasi-conformal mapping," *Progress In Electromagnetics Research*, Vol. 13, 261–273, 2010.
22. Pendry, J. B., A. Holden, W. Stewart, and I. Youngs, "Extremely low frequency plasmons in metallic mesostructures," *Physical Review Letters*, Vol. 76, No. 25, 4773, 1996.
23. Pendry, J. B., A. J. Holden, D. J. Robbins, and W. Stewart, "Magnetism from conductors and enhanced nonlinear phenomena," *IEEE Transactions on Microwave Theory and Techniques*, Vol. 47, No. 11, 2075–2084, 1999.
24. Pedrola, G. L., *Beam Propagation Method for Design of Optical Waveguide Devices*, John Wiley & Sons, 2015.
25. Basser, J., J. Mattiello, and D. LeBihan, "Mr diffusion tensor spectroscopy and imaging," *Biophysical Journal*, Vol. 66, No. 1, 259–267, 1994.

26. Nye, J. F., *Physical Properties of Crystals: Their Representation by Tensors and Matrices*, Oxford University Press, 1985.
27. Kuprel, B. and A. Grbic, "Anisotropic inhomogeneous metamaterials using nonuniform transmission-line grids aligned with the principal axes," *IEEE Antennas and Wireless Propagation Letters*, Vol. 11, 358–361, 2012.
28. Lam, T. A., D. C. Vier, J. A. Nielsen, C. G. Parazzoli, and M. H. Tanielian, "Steering phased array antenna beams to the horizon using a buckyball nim lens," *Proceedings of the IEEE*, Vol. 99, No. 10, 1755–1767, 2011.
29. Ansys, H., "v15," *ANSYS Corporation Software*, Pittsburgh, PA, USA, 2014.
30. Smith, D. R., S. Schultz, Markoš, and C. Soukoulis, "Determination of effective permittivity and permeability of metamaterials from reflection and transmission coefficients," *Physical Review B*, Vol. 65, No. 19, 195104, 2002.
31. Chen, X., T. M. Grzegorzczak, B.-I. Wu, J. Pacheco, Jr, and J. A. Kong, "Robust method to retrieve the constitutive effective parameters of metamaterials," *Physical review E*, Vol. 70, No. 1, 016608, 2004.
32. Liu, R., T. J. Cui, D. Huang, B. Zhao, and D. R. Smith, "Description and explanation of electromagnetic behaviors in artificial metamaterials based on effective medium theory," *Physical Review E*, Vol. 76, No. 2, 026606, 2007.
33. Smith, D., D. Vier, T. Koschny, and C. Soukoulis, "Electromagnetic parameter retrieval from inhomogeneous metamaterials," *Physical review E*, Vol. 71, No. 3, 036617, 2005.
34. Barton, J. H., C. R. Garcia, E. A. Berry, R. Salas, and R. C. Rumpf, "3-d printed all-dielectric frequency selective surface with large bandwidth and field of view," *IEEE Transactions on Antennas and Propagation*, Vol. 63, 1032–1039, March 2015.
35. Fraser, A. S., "Simulation of genetic systems by automatic digital computers vi. epistasis," *Australian Journal of Biological Sciences*, Vol. 13, No. 2, 150–162, 1960.
36. Clerc, M., *Particle Swarm Optimization*, John Wiley & Sons, Vol. 93, 2010.
37. Rumpf, R. C., C. R. Garcia, E. A. Berry, and J. H. Barton, "Finite-difference frequency-domain algorithm for modeling electromagnetic scattering from general anisotropic objects," *Progress In Electromagnetics Research*, Vol. 61, 55–67, 2014.
38. Rumpf, R. C. and J. Pazos, "Synthesis of spatially variant lattices," *Optics Express*, Vol. 20, No. 14, 15263–15274, 2012.
39. Rumpf, R. C., "Engineering the dispersion and anisotropy of periodic electromagnetic structures," *Solid State Physics*, Vol. 66, 213–300, Elsevier, 2015.
40. Rumpf, R. C., J. Pazos, C. R. Garcia, L. Ochoa, and R. Wicker, "3d printed lattices with spatially variant self-collimation," *Progress In Electromagnetics Research*, Vol. 139, 1–15, 2013.
41. Rumpf, R. C., J. J. Pazos, J. L. Digaum, and S. M. Kuebler, "Spatially variant periodic structures in electromagnetics," *Philosophical Transactions of the Royal Society A: Mathematical, Physical and Engineering Sciences*, Vol. 373, No. 2049, 20140359, 2015.
42. Greville, T., "Some applications of the pseudoinverse of a matrix," *SIAM review*, Vol. 2, No. 1, 15–22, 1960.
43. Noble, B. and J. W. Daniel, *Applied Linear Algebra*, 3rd Edition, Prentice Hall, 1988.
44. Sacks, Z. S., D. M. Kingsland, R. Lee, and J.-F. Lee, "A perfectly matched anisotropic absorber for use as an absorbing boundary condition," *IEEE Transactions on Antennas and Propagation*, Vol. 43, No. 12, 1460–1463, 1995.